AIAA JOURNAL
Vol. 44, No. 5, May 2006

Particle Response to Low-Reynolds-Number Oscillation of a Fluid in Microgravity

Drew L'Espérance* and James D. Trolinger†
MetroLaser, Inc., Irvine, California 92614
Carlos F. M. Coimbra‡
University of Hawaii–Manoa, Honolulu, Hawaii 96822
and
Roger H. Rangel§
University of California, Irvine, Irvine, California 92697

This works presents an experimental study on the response of a particle to the movement of the fluid in which the particle is suspended. The stationary solution to Tchen's equation of motion was used to design experiments to determine the influence of the Basset history force. In the experiments, the stationary amplitude ratio and phase difference between the fluid and the particle motion are measured in a fluid cell containing a particle that is supported by a tether to counteract the effect of gravity. Particle and cell locations at the limits of motion are measured with great precision by applying electronic holography. The measured particle responses closely match the theoretical predictions for the full solution for a variety of fluid-to-particle density ratios, Reynolds numbers, and frequencies of oscillation. The experiments reinforce the importance of the Basset history term for moderate to high-frequency flows.

I. Introduction

THE fundamental problem of the motion of a particle suspended in a viscous fluid is relevant to many scientific and engineering applications ranging from crystal growth in microgravity environments to particle dispersion in turbulent flows. The ground experimental results described in this work are in support of a planned spaceflight project, SHIVA (Spaceflight Holography Investigation in a Virtual Apparatus), and emphasize the most current understanding of the influence of history drag forces on the motion of small particles in suspension.[1] Among the various predictions that can be made, the most recent theoretical advances have helped us design experiments that have produced a better understanding of the significance of the most evasive term in the equation, known as the Basset history force. The objectives of the ground-based study presented in this paper are to compare experimental results with the stationary solution to the particle equation of motion and to provide support to a planned spaceflight microgravity experiment in which the equation of motion can be fully tested under transient conditions.

This work utilized both experiment and theory to identify and resolve critical issues to produce an optimal experiment design that exploits microgravity for the study. We examined the response of heavy and light particles to fluid oscillation at frequencies where the Basset history force is one of the most predominant forces acting on the particle. The particle sizes and velocities used corresponded to the low particle Reynolds number ($Re_p < 1$) and high-Strouhal–Reynolds ($S = Sl\,Re_p$) regimes. To observe some of the interesting effects predicted by the new solutions requires the precise location of the position of a particle in three dimensions. To this end, we have developed digital holography algorithms that enable particle position location to a small fraction of a pixel in a charge-coupled-device (CCD) array. The experiments provide a definitive, quantitative observation of the Basset history force over a wide range of experimental conditions.

II. Background

Tchen[2] derived a Lagrangian equation of motion for a spherical particle freely moving in a uniform, time-dependent background flow as a culmination of previous work attributed to Boussinesq,[3] Basset,[4] and Oseen.[5] Coimbra and Rangel[1] recognized that Tchen's equation could be written in terms of fractional derivatives and used fractional calculus to solve Tchen's equation for a generic forcing function that included both gravitational and fluid acceleration contributions. In terms of the relative velocity $w = v - u$, where v and u are the particle and fluid velocity, respectively, Tchen's equation is written as

$$\frac{\mathrm{d}w}{\mathrm{d}\hat{t}} + 3\frac{\alpha}{\alpha+2}\frac{\mathrm{d}^{\frac{1}{2}}w}{\mathrm{d}\hat{t}^{\frac{1}{2}}} + \frac{\alpha}{\alpha+2}w = \frac{\alpha}{\alpha+2}G + 2\frac{\alpha-1}{\alpha+2}\frac{\mathrm{d}u}{\mathrm{d}\hat{t}} \qquad (1)$$

where α is the ratio of the fluid density to the particle density. The dimensionless time $\hat{t}$ is equal to the actual time divided by the viscous timescale τ_f given by $a^2/9\nu$, where a is the particle radius and ν is the kinematic viscosity of the fluid. The gravitational coefficient G is equal to $(1-\alpha)\tau_f g$, where g is the local gravity acceleration (typically a negligible contribution in microgravity environments).

The first term in Eq. (1) corresponds to the relative acceleration corrected by a virtual mass coefficient $(\alpha+2)/\alpha$, which affects all of the other terms in the equation. The third term in Eq. (1) is proportional to the relative velocity whereas the second (half-derivative) term has an intermediate dependence that is dynamically proportional to both the relative velocity and acceleration. Before the work of Coimbra and Rangel,[1] the dimensionless Basset drag (second term of the equation) had been expressed in integral form only and thus was responsible for the integro-differential nature of the particle equation of motion. Because integro-differential equations are typically much more difficult to treat both analytically and numerically than ordinary differential equations, the history drag has been neglected in the majority of past particle motion studies.

Presented as Paper 2004-1147 at the AIAA 42nd Aerospace Sciences Meeting, Reno, NV, 5–8 January 2004; received 1 March 2004; revision received 21 March 2005; accepted for publication 18 April 2005.

*Senior Scientist, 2572 White Road.
†Vice President and Director of Research, 2572 White Road. Senior Member AIAA.
‡Associate Professor, Department of Mechanical Engineering. Associate Member AIAA.
§Professor, Department of Mechanical and Aerospace Engineering. Member AIAA.

Particle motion in oscillating flows has generated a significant amount of research activity. One practical example of particle motion in oscillating flows is that of a crystal suspended in a fluid subject to mechanical vibration. In harmonically oscillating flows, neither the particle velocity nor the particle acceleration reaches a steady-state value, and all three terms on the left side of Eq. (1) affect the particle motion, particularly at moderate to high frequencies ($S \sim 1$). Coimbra and Rangel[6] applied the general solution of Tchen's equation,[1] including the initial transients and influence of gravity, to the case of a spherical particle responding to a sinusoidal background flow at low Reynolds number. In the following paragraphs, we summarize the main features of the solution when applied to the simpler case of stationary sinusoidal motion in the absence of gravity, a case that has been studied with varying degrees of sophistication over the past 40 years by many different authors.[7–13] Coimbra et al.[7] provide a more extensive review of previous works in the area.

For our experiments, it suffices to let the background velocity of the fluid (i.e., velocity of the fluid far away from the particle) be represented by $u = A\exp(i\Omega t)$, where A is the velocity amplitude and Ω is the angular frequency of oscillation. In the steady-state case, the particle responds by oscillating sinusoidally with a velocity given by $v = B\exp(i\Omega t + i\phi)$, where B is the particle velocity amplitude and ϕ represents the phase difference between the particle motion and fluid motion. We wish to find the response coefficient η, which is given by Eq. (2):

$$\eta \equiv (B/A)\exp(i\phi) \tag{2}$$

To facilitate comparisons between particles of different sizes and fluids of varying viscosity, it is useful to define a dimensionless frequency S (Ref. 7):

$$S = \Omega\tau_f = \Omega a^2/9\nu \tag{3}$$

The fluid velocity, particle velocity, and relative velocity are expressed in terms of η and S by Eqs. (4a–4c):

$$u = A\exp(iS\hat{t}) \tag{4a}$$

$$v = \eta u \tag{4b}$$

$$w = v - u = (\eta - 1)u \tag{4c}$$

Substitution of expressions (4a–4c) into Eq. (1), followed by solving for η, gives[9]

$$\eta(S,\alpha) = 1 + \frac{i2S(\alpha - 1)}{iS(\alpha + 2) + \alpha + 3\alpha\sqrt{S}\exp(i\pi/4)} \tag{5}$$

The ratio of velocity amplitudes is equal to the ratio of displacement amplitudes. The last term in the denominator of Eq. (5) (i.e., the term proportional to $\sqrt{S}$) is as a result of the history drag and is the dominant term when $S \approx 1$.

III. Experiments

Because the movement of a spherical particle in response to the surrounding fluid is predicted by Eq. (5), we tested the theory by measuring the response of the particle to the fluid motion. Specifically, we measured the ratio of the particle A_p to fluid cell A_c displacement amplitudes at different forcing frequencies. The particle and cell displacements were measured by recording two in-line holograms at the extremes of the cell displacement. Because of the phase difference ϕ between the particle motion and the fluid motion, the measured particle displacement A'_P is equal to $A_p\cos\phi$, and the ratio of A'_P to A_c is equal to the real component of η [Eq. (6)]:

$$A'_P/A_C = Re(\eta) = |\eta|\cos\phi \tag{6}$$

The investigation focused on particles in fluids oscillating at dimensionless frequencies S between 0.1 and 6, where the history drag is dominant, moving at particle Reynolds numbers less than 1.

Table 1 Material properties

Material	Density, g/cm^3	Viscosity, cm^2/s
Krytox	1.91	0.40
Krytox + DFP	1.77	0.27
Mineral oil	0.86	1.85
Polypropylene	0.91	——
Mg alloy	1.77	——
Brass	8.67	——

A. Particles and Fluid Cell

The properties of the particles and fluids used in the experiment are given in Table 1. Krytox (perfluoroalkylether) and mineral oil were used as fluids in the experiment because they are transparent and have low flammability, low toxicity, and high viscosity. To test the influence of the particle-to-fluid-density ratio on particle motion, two different cases were examined: a light spherical particle (polypropylene in Krytox, $\alpha = 2.1$) and a heavy spherical particle (brass in mineral oil, $\alpha = 0.1$). To prevent the particles from floating or sinking, 2-cm-long tethers made from 19-μm-diam copper wires were used to anchor the particles to either the bottom or top of the cell. A control experiment at $\alpha = 1.0$ was performed using neutrally buoyant magnesium alloy spheres suspended without tethers in a solution of Krytox plus decafluoropentane (DFP).

In Krytox, the frequencies corresponding to $S = 1$ are 57.3 Hz for $a = 1$-mm spheres and 14.3 Hz for $a = 2$-mm spheres. In mineral oil, which is more viscous, the frequency corresponding to $S = 1$ is 66.2 Hz for an $a = 2.0$-mm sphere. The shaker used to oscillate the fluid-filled cell is described in Ref. 14.

B. Measuring the Cell and Particle Position

The cell was illuminated using a defocused, collimated beam from a helium–neon laser. In-line holograms of the particle and a reference marker glued to the cell window were recorded using a lens-less CCD camera located between 10 and 20 cm behind the cell. A shutter in front of the laser was triggered to open for 0.8 ms at the two extremes of a cell oscillation cycle when the cell velocity was zero. The camera was operated in double-exposure mode and synchronized with the shutter, resulting in two images of the cell at the two extremes of cell motion.

The CCD camera was positioned such that a bright spot, known as the Arago spot (also called the Poisson spot), formed in the center of the diffracted shadows of the particle and cell reference particle.[15] The Arago spot and its surrounding rings provided an excellent noise-free, predictable light pattern. Cell and particle positions were determined from the in-line holograms by cross correlating the holograms with an analytically generated template of the Arago spot and surrounding rings. For the region of the shadow within half a radius of the center, the intensity $I(x, y)$ of a pixel with coordinates (x, y) is approximated by Eq. (7):

$$I(x, y) = I_0 J_0^2\left(\pi\sqrt{(x - x_0)^2 + (y - y_0)^2}\Big/\sigma\right) \tag{7}$$

where I_0 is the intensity of the center of the Poisson spot; J_0 is the zeroth-order Bessel function; x_0, y_0 are the coordinates of the pattern center; and σ is the ring spacing in pixels. The ring spacing depends upon the particle radius a, the distance between the camera and particle z, the wavelength of light used λ, and the length of each pixel s [Eq. (8)]:

$$\sigma = \lambda z/2as \tag{8}$$

The ring spacing of the particle was computed by locating the brightest pixel in the center of the particle shadow, calculating the average radial intensity distribution $I(r)$ centered on this pixel, then using the Levenberg–Marquardt method to find the best fit of Eq. (7) to the radial intensity distribution with I_0 and σ as adjustable parameters (Fig. 1). The same method was used to find the ring spacing of the cell marker.

Once the ring spacing of the particle and cell marker were determined, a template image was generated in the form of Eq. (7). The

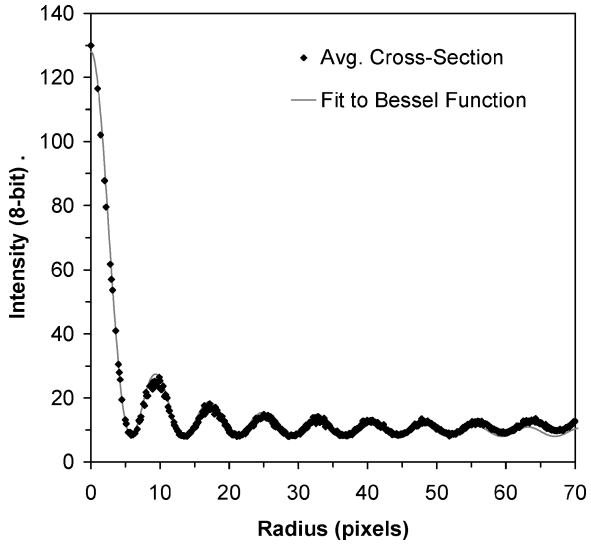

Fig. 1 Plot of experimental radial distribution function [$I(r)$ vs r].

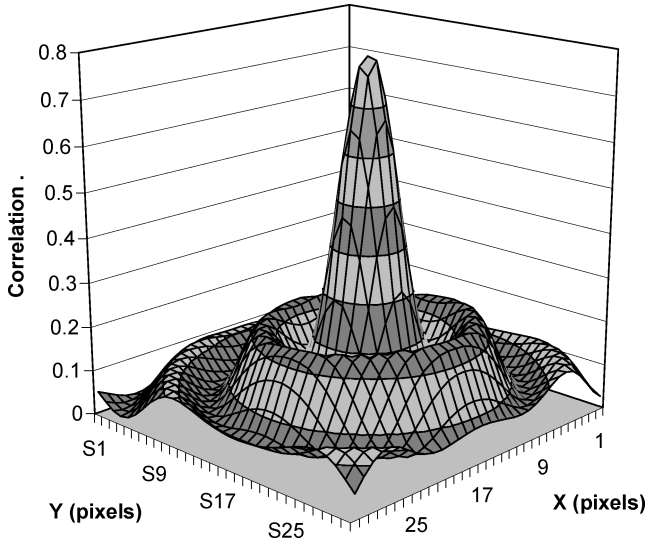

Fig. 2 Surface plot of 32 × 32 central pixels of the cross-correlation function.

size of the template was limited to approximately the region within half the radius of the particle or cell marker. Ideally, the template represents the pattern of rings as it would appear if the noise, which is not circularly symmetric, were averaged out.

During a typical experiment, batches of 70 or more images of a single tethered particle were recorded, all having the same ring spacing. Therefore, we determined the average ring spacing for four sample images, generated the template corresponding to this ring spacing, and used the template to analyze every image in the batch. The images were analyzed by extracting a square region of interest near the center of the particle shadow to make a source image equal in size to the template, then computing the cross correlation $\boldsymbol{X}$ of the source $\boldsymbol{S}$ and template $\boldsymbol{T}$ according to Eq. (9):

$$\boldsymbol{X} = \text{Real}\{\Im^{-1}(\Im\boldsymbol{T} \cdot \Im\boldsymbol{S})\} \tag{9}$$

The maximum of the cross correlation (Fig. 2) corresponds to the position where the template best overlaps the source image and should also correspond to the true center of the particle.

The particle and cell positions or amplitudes must be determined with an accuracy of 5 μm. It would be beneficial to do better than this, say, 1–2 μm. Because the pixels are 9 μm in length, we developed an interpolation procedure to locate the cross-correlation peak to subpixel resolution. The procedure extracts two five-pixel arrays,

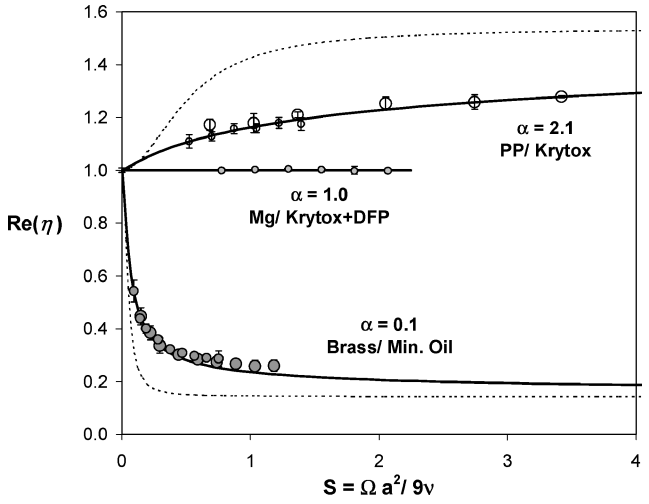

Fig. 3 $Re(\eta)$ vs S for particles at three different relative densities: —— curves, predicted response with history effects; and - - - - curves, response without history effects.

one vertical and the other horizontal, centered about the pixel with the maximum correlation value. The correlation intensities of each five-pixel array were then plotted vs position and fit by a parabola. The vertices of the parabola correspond to the coordinates of the cross-correlation peak.

We tested the program by constructing synthetic images of a particle upon a noisy background, where the particle center was known. The program was able to locate the center of the particles to within 0.1 pixel or better. In another test, we used a micrometer to displace a fixed particle by amounts ranging from 88 to 108 μm. Comparison between the mechanically measured and optically measured displacement confirmed that the particle could be located to a precision of at least 0.1 pixel, or 1 μm.

IV. Results

A. Experiments at Low Reynolds Number

Figure 3 shows a plot of the experimentally measured particle response $Re(\eta)$ vs dimensionless frequency for polypropylene particles in krytox ($\alpha = 2.1$), magnesium alloy particles in Krytox + DFP ($\alpha = 1.0$), and brass particles in mineral oil ($\alpha = 0.1$). Two different-sized polypropylene particles were used, one with a radius of 1.00 mm and the other with a radius of 1.98 mm. Two different-sized brass particles were used, one with a radius of 1.59 mm and the other with a radius of 1.98 mm. The magnesium particle had a radius of 1.00 mm. The uncertainty bars in the figure represent the 95% confidence limit.

Also shown on the figure are the theoretically predicted response curves with the history term included (solid bold curves) and neglected (thin dashed curves). For both the heavy and light particles, the data closely match the theoretically predicted response curves where history effects are included, and the experimental uncertainty is much less than the difference between the history and no-history effect curves. In the case of $\alpha = 1$ particles, the theory predicts a response coefficient of $\eta = 1$ at all frequencies and that the history drag has no effect.

B. Experiments at Higher Particle Reynolds Numbers

We investigated the effect of particle Reynolds number on the response of heavy particles to cell motion by examining a 1.98-mm-radius brass sphere in krytox ($\alpha = 0.22$). The experiments were carried out at a cell oscillation frequency of 14.9 Hz, at which frequency the dimensionless frequency $S = 1.02$. The particle Reynolds number was varied by adjusting the cell amplitude A_c; the particle Reynolds number can be determined from the cell amplitude and magnitude of the displacement ratio, according to Eq. (10):

$$Re_p = a|W|/\nu = 9SA_c(1 - |\eta|)/a \tag{10}$$

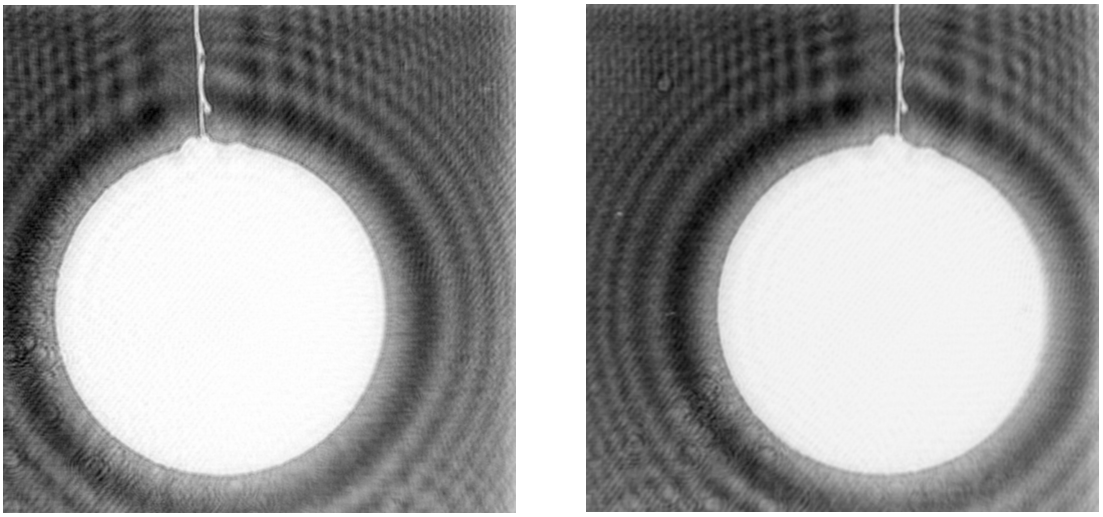

a) Left extreme **b) Right extreme**

Fig. 4 Reconstructed image of tethered brass particle at two extreme positions.

Table 2 Results from $a = 1.98$-mm particle, $\alpha = 0.22$, oscillating at $S = 1.02$

A_c, μm	Re_p	$\lvert\eta\rvert$	ϕ, deg
317	0.78	0.471	−19
636	1.56	0.471	−19
907	2.22	0.473	−19
1322	3.23	0.474	−19

Table 3 Results from $a = 1.98$-mm particle, $\alpha = 2.1$, oscillating at $S = 1.02$

A_c, μm	Re_p	$\lvert\eta\rvert$	ϕ, deg
181	0.14	1.170	+6.4
375	0.30	1.173	+6.4
524	0.41	1.170	+6.4
782	0.62	1.170	+6.4
1060	0.84	1.170	+6.4
1347	1.06	1.169	+6.4

For this part of the investigation, we collected a series of images at different phases of the cell motion so that A_p, A_c, η, and ϕ could be measured directly. This was accomplished by leaving the shutter open, setting the camera exposure time to 0.1 ms, and triggering the camera by a pulse generator synchronized to the voice coil driver signal. A series of 75 images were recorded at 3-s intervals with the delay between the driver signal and the trigger pulse varied between images; the delay was typically varied over a range covering two periods of the cell oscillation. The disadvantage of this triggering method is that the images are collected over a relatively long time (about 3 min), so that the measured cell and particle positions must be corrected to account for small low-frequency vibrations that cause the cell zero position to drift. The positions of the test cell and particle as a function of time delay were fit by sine waves to determine A_p, A_c, and ϕ.

The results for oscillation of the brass particle at four different particle Reynolds numbers are given in Table 2. The results show that $|\eta|$ and ϕ are nearly constant over particle Reynolds numbers ranging from 0.8 to 3.2. The results are very close to the theoretically predicted values for $S = 1.02$ and $\alpha = 0.22$ at low Reynolds number, which are $|\eta| = 0.474$ and $\phi = -17$ deg. If history effects are neglected, the theory predicts $|\eta| = 0.311$ and $\phi = -12.5$ deg.

We performed virtually the same experiment with a 1.98-mm polypropylene particle in Krytox ($\alpha = 2.1$) with Re_p ranging from 0.14 to 1.06. The results are presented in Table 3. Once again, the values of $|\eta|$ and ϕ are nearly constant over the Re_p range and are close to the theoretically predicted values with history included ($|\eta| = 1.170$ and $\phi = +6.1$ deg), but very different from the predicted values where history is neglected ($|\eta| = 1.443$ and $\phi = +8.5$ deg).

C. Tether Effects

To examine the effects of tethers on the particle motion more closely, we reconstructed images from the in-line holograms. The digital reconstruction process is described in Ref. 16. Two reconstructions of a tethered 1.98-mm-radius brass particle, one taken at the left extreme of particle motion and the other at the right extreme, are shown in Fig. 4. The images show that as the particle moves it pivots about the tether attachment point. The result is that the particle rotates about 10 deg, while the tether swings through an angle of about 3 deg. The effect is especially noticeable when the series of images are animated.

The pivoting motion of the particle might explain some of the discrepancies between the experimental data from brass particles and the theoretical curves seen in Fig. 3. For both sizes of brass particles, the difference between the experimental data and the theoretical curves increases as the cell frequency increases. Because the velocity of the particle is proportional to the cell frequency, increasing the oscillation frequency increases the particle velocity for a fixed amplitude. The pivoting motion of the particle should increase as the particle velocity increases. We did not observe this tether effect in our experiments with tethered polypropylene particles.

V. Conclusions

In the foregoing, we have presented some results of a ground-based experimental program that is designed to support the flight experiment SHIVA. Using a tethered particle method to simulate microgravity, we conducted a range of experiments, identified and resolved what appear as the most challenging obstacles to a successful experiment, and developed the necessary methods to meet experiment goals.

The results show that the tethered particle method is a viable experimental method for ground experiments, and the data are largely consistent with theoretical predictions provided that the particles are not too small. The results also suggest that Tchen's equation can also apply for particle Reynolds numbers up to 3 for values of S of order 1.

Acknowledgments

This work is supported by NASA's flight definition project SHIVA (Spaceflight Holography Investigation in a Virtual Apparatus) under Contract NAS8-98091. The NASA management team includes M. Bodiford, Project Manager; D. Smith, Project Scientist;

and W. Patterson, Systems Engineer, all from NASA's Marshall Space Flight Center. The authors acknowledge M. Dempsey of MetroLaser for conducting much of the experimental work.

References

[1]Coimbra, C. F. M., and Rangel, R. H., "General Solution of the Particle Momentum Equation in Unsteady Stokes Flow," *Journal of Fluid Mechanics*, Vol. 370, 1998, pp. 53–72.

[2]Tchen, C. M., "Mean Value and Correlation Problems Connected with the Motion of Small Particles Suspended in a Turbulent Fluid," Ph.D. Dissertation, Dept. of Physics, Delft Univ., The Hague, The Netherlands, July 1947.

[3]Boussinesq, J., "Sur la Résistance qu'Oppose un Liquide Indefini en Repos, sans Pesanteur, au Mouvement Varié d'une Sphère Solide Qu'il Mouille sur Toute sa Surface, Quand les Vitesses Restent Bien Continues et Assez Faibles pour que Leurs Carrés et Produits Soient Negligeables," *Comptes Rendus Academie Sciences Paris*, Vol. 100, Dec. 1885, pp. 935–937.

[4]Basset, A. B., "On the Motion of a Sphere in a Viscous Liquid," *Philosophical Transactions of the Royal Society of London A*, Vol. 179, Nov. 1888, pp. 43–63.

[5]Oseen, C., *Hydromechanik*, Akademische Verlag, Leipzig, Germany, 1927.

[6]Coimbra, C. F. M., and Rangel, R. H., "Spherical Particle Motion in Harmonic Stokes Flows," *AIAA Journal*, Vol. 39, No. 9, 2001, pp. 1673–1682.

[7]Coimbra, C. F. M., L'Esperance, D., Lambert, R. A., Trolinger, J. D., and Rangel, R. H., "An Experimental Study on Stationary History Effects in High Frequency Stokes Flows," *Journal of Fluid Mechanics*, Vol. 504, 2004, pp. 353–363.

[8]Corrsin, S., and Lumley, J., "On the Equation of Motion for a Particle in Turbulent Fluid," *Applied Science Research*, Vol. 6, No. 5, 1956, pp. 114–116.

[9]Hinze, O., *Turbulence*, 2nd ed., McGraw–Hill, New York, 1975, Chap. 5, pp. 460–471.

[10]Hjelmfelt, A. T., and Mockros, L. F., "Motion of Discrete Particles in Turbulent Fluid," *Applied Science Research*, Vol. 16, April 1996, pp. 148–161.

[11]Morrison, F. A., and Stewart, M. B., "Small Bubble Motion in an Accelerating Fluid," *Journal of Applied Mechanics*, Vol. 97, June 1976, pp. 399–402.

[12]Chao, B. T., "Turbulent Transport Behavior of Small Particles in Dilute Suspension," *Österreichisches Ingenieur-Archiv*, Vol. 18, Aug.–Nov. 1968, pp. 7–21.

[13]Friedlander, S. K., "Behavior of Suspended Particles in a Turbulent Fluid," *American Institute of Chemical Engineering Journal*, Vol. 3, No. 3, 1957, pp. 381–388.

[14]Trolinger, J. D., L'Esperance, D., Rangel, R. H., Coimbra, C. F. M., and Witherow, W. K., "Design and Preparation of a Particle Dynamics Space Flight Experiment, SHIVA," *Annals of the New York Academy of Science*, Vol. 1027, Nov. 2004, pp. 550–566.

[15]Harvey, J. E., and Forgham, J. L., "The Spot of Arago: New Relevance for an Old Phenomenon," *American Journal of Physics*, Vol. 52, No. 3, 1984, pp. 243–247.

[16]Vikram, C. S., *Particle Field Holography*, Cambridge Univ. Press, Cambridge, England, U.K., 1992, Chap. 3.

R. Lucht
Associate Editor